Development of a turbulent liquid flux model for Eulerian-Eulerian multiphase flow simulations

https://doi.org/10.1016/j.ijmultiphaseflow.2016.02.003

Development of a turbulent liquid flux model for Eulerian-Eulerian multiphase flow simulations

Antonio Andreini, Cosimo Bianchini, Stefano Puggelli

Department of Industrial Engineering, University of Florence, Via di Santa Marta 3 - 50139, Florence, Italy

F.X. Demoulin

CNRS CORIA UMR 6614, University of Rouen, Technopôle du Madrillet, BP 12, 76801 Saint-Etienne-du-Rouvray Cedex, France

Abstract

The present work introduces a multiphase Eulerian solver, developed in the framework of the CFD suite OpenFOAM, aimed at including all the major physical phenomena that characterize liquid fuel atomization. The study begins with the Eulerian solver derived from the Eulerian Lagrangian Spray Atomization (ELSA) model (Borghi and Vallet, 1999; Vallet et al., 2001). This approach is suitable to describe the liquid-gas flow for all liquid volume fraction from bubbly, dense to spray flows without any assumption on the topology of the phase (droplets, bubbles, ligaments or any continuous structures). However, due to its single phase flow formalism, the slip velocity between phases is hidden in the *turbulent liquid flux* term inside the liquid volume fraction equation. An innovative second order closure for this variable is here proposed and implemented. A detailed analysis of the resulting Quasi-Multiphase Eulerian (QME) solver capabilities is performed in RANS context exploiting a jet in crossflow test case with available experimental and computational data. The test is extremely challenging as it involves a high density ratio (R) (i.e. two cases at R=10 and R=1000 were simulated) and it explores the entire range of liquid phase concentration from purely liquid to dispersed phase. The comparison with the experimental results shows that the proposed approach leads to a comprehensive and physically consistent description of the phenomena related to liquid injection.

1. INTRODUCTION

With the increasing demand for air transportation for civil purpose, large research efforts have been devoted to reduce the negative environmental effects of civil aviation. This is confirmed by both ACARE 2020 objectives and ICAO-CAEP standards (ICAO, 2010) that impose NO_x emission abatement as one of the main goal in the development of next aero-engine generation. In this context, the analysis and the optimization of the combustion system is surely one of the key aspects. Even though RQL (*Rich Quench Lean*) concept still offers relevant prospects for development, huge research efforts have been prompted in last years towards the introduction of lean burn combustion systems, already adopted in heavy-duty gas turbines in last 20 years. Thus, a significant portion of investigations in the lean combustion field has been devoted towards the development of advanced injection systems committed to enhance the fuel/air mixing and to ensure a fine atomization.

Hence, several example of lean burn injectors have been developed in the last years (Meier et al., 2013; Mongia, 2003; Buelow et al., 2006; Hernandez et al., 2015). The Injector exploited in the GE-TAPS (*Twin Annular Premixing Swirler*) combustor, which currently represents the only lean burn combustion system employed on a certified aircraft engine (GEnX family), is particularly relevant (Mongia, 2003; Li et al., 2010; Cooper et al., 2002; Foust and Mongia, 2007). Figure 1 shows a schematic representation of this configuration which is based on an internally staged pilot in-

*Stefano Puggelli
Email address: stefano.puggelli@htc.de.unifi.it (Stefano Puggelli)

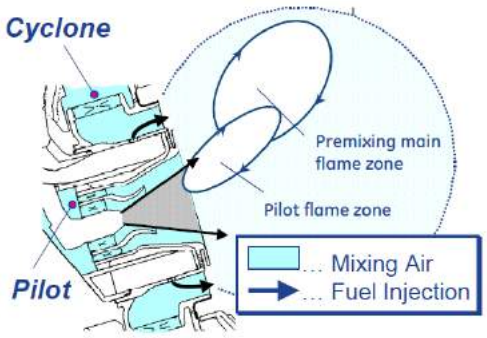

Figure 1: TAPS internally staged fuel injector concept (Mongia, 2003).

jector with a lean direct multi-point injection for the main stage operation. The pilot consists in a pressure atomizer surrounded by two co-rotating swirlers whereas the main mixer consists of a radial inflow swirler (cyclone) and a cavity where the fuel is injected through a series of transverse jets (Cooper et al., 2002).

As an alternative to the mentioned discrete jets atomization process, a common approach is to adopt liquid film atomization by means of prefilming airblast atomizers. An intersting solution employing this concept is the so-called PERM (*Partially Evaporating and Rapid Mixing*) injection system developed by Avio Aero (Marinov et al., 2010; Kern et al., 2011). The injector is a double swirler airblast atomizer developed in order to achieve partial evaporation inside the inner duct and rapid mixing within the combustor, optimising the location and the stability of the flame as sketched in Figure 2. A film of fuel is generated over the inner surface of the lip that separates the two swirled flows. As the film reaches the edge of the lip, through the action of the gas flow, primary atomization occurs: fine droplets and rapid mixing are promoted by the two co-rotating swirled flows generated by the double swirler configuration. Furthermore, in order to ensure a stable operation of the flame, especially at low power conditions, the airblast injector is coupled with a hollow cone pressure atomizer (pilot injector), located at the centre of the primary swirler, which generates a pilot flame to stabilize the combustion process in a configuration similar to a piloted airblast atomizer.

Considering these complex flowfield features with a high coupling level between liquid and gas phase, in order to integrate the information obtained by experimental campaigns in highly pressurized reactive environments, numerical modelling has continuously gained importance for design scopes over the last years.

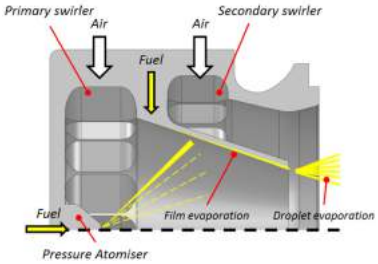

Figure 2: PERM functioning concept (Andreini et al., 2014b).

Typical industrial simulations are usually performed with a Reynolds Average Navier Stokes (RANS) approach and, in this context, the Eulerian-Lagrangian methods, where the gas phase is modelled in an Eulerian framework and the liquid is tracked with a Lagrangian description as composed by discrete entities (i.e. *parcels*), are widely employed since they have shown good capabilities in predicting the most important flow structures and interactions between the two phases (Andreini et al., 2014a, 2013; Chrigui et al., 2008; Ruger et al., 2000). Such approaches allow a straightforward implementation of physical processes such as evaporation, secondary break-up and poly-dispersion even if their computational costs are normally huge because of the number of parcels normally needed in each cell of the computational domain in order to have a statistically representative solution. This feature has become more restrictive considering that the unsteady evolution of lean spray flames normally requires an extensive use of unsteady and scale resolved approaches (Gicquel et al., 2012) where costs of Eulerian-Lagrangian methods rapidly grow above the usual affordable levels for industrial applications (Lavergne, 2012; Laurent and Massot, 2001). Indeed, it should be considered that, due to the coupling between a continuous and a discrete phase, the opportunities of numerical vectorization and parallelization, normally adopted in single-phase simulations, are very limited involving large computational requirements in the context of complex geometries like aeroengine combustors.

These shortcomings make the Eulerian-Eulerian approaches very attractive for the description of the spray characteristics. Here, the starting point is

to consider the two phase flows at the mesoscopic level: at this level, the spray is considered as a set of droplet and the evolution in time of the characteristics of each droplet (i.e. position, velocity or diameter) has its proper model similar to those exploited in the Lagrangian framework. From these bases, it is possible to derive a transport equation for the spray distribution which describes the joint probability function for such characteristics. This general equation is referred as the kinetic Boltzmann-Williams (Williams, 1958).

It is worth noting that the Lagrangian approach for the spray corresponds to a Monte-Carlo resolution of this equation using a stochastic method. Eulerian approaches for the spray modelling attempt to solve the Boltzmann-Williams equation within an Eulerian framework based on the Euler description of the carrier phase. The growing attention for such approaches is due to their benefits in terms of numerical efficiency, which become extremely important in the context of Large Eddy Simulation (LES). Nevertheless, despite the efficiency of Eulerian methods on actual HPC clusters, the direct resolution of the spray distribution is generally not feasible since the dimension of the problem is increased by the number of spray characteristics retained. This constrains the Eulerian method to address a limited description of the spray distribution.

The different hypothesis exploited in order to simplify the spray distribution has led to an abundant research on spray Eulerian methods. The first method consist in the reduction of the dimension of the problem by selecting some spray characteristics, such as the diameter. In this case the distribution is discretized along the diameter space leading to a particular class of method called the *sectional approach* (Laurent and Massot, 2001; Laurent et al., 2004). This method is relevant if all the spray characteristics (e.g. velocity and temperature) are mainly driven by the diameter. Furthermore, It presents the main advantage of avoiding any assumption on the size distribution of the spray even if it has an important computational cost because there is still another dimension to solve in addition to space and time.

Another widely exploited class of method is based on computing only given moment of the spray probability density function. For instance, it is possible to integrate the Boltzmann-Williams equation to get mean characteristics of the spray as mean number density or mean diameter. To improve such description, other moments can be added with their corresponding equation obtained from the integration of the Boltzmann-Williams equation and of the spray distribution (Boivin et al., 2000; Simonin, 2000; Riber et al., 2006). If a Gauss quadrature method is used to integrate such term, the problem is closed as soon as the Gauss points and their weights are known. The so called QMOM (*Quadrature Method of Moments*) approach considers a number of quadrature points that can be fully determined by the definition of moments. The accuracy of the method in principle increases with the number of Gauss quadrature points available thus with the number of moments retained. Some difficulties arise in finding the quadrature points from the known moments because it requires the resolution of a nonlinear set of equations. To avoid this problem the DQMOM (*Direct Quadrature Method of Moments*) method has been proposed where the transport equations concern directly the characteristics of Gauss quadrature points instead of the moments of the distribution (McGraw, 1997; Marchisio et al., 2003; Marchisio and Fox, 2005; Fox et al., 2008).

From this discussion it is clear that Eulerian approaches for spray are very valuable in comparison to the full stochastic Lagrangian methods because it is possible to choose the level of detail used to represent the spray distribution. However, if the spray distribution is completely unknown without any particular characteristic, it is necessary to completely solve it and the Lagrangian method is normally the most suitable choice. Furthermore, all the previously described methods are based on the Boltzmann-Williams equation, thus the spray should be composed of individual droplets with well-defined features such as position or diameter. Neverthless, during the process of atomization the liquid phase is initially a continuum such as a liquid jet or film and it is not possible to define such characteristics.

To overcome such limitations, an Eulerian solver able to include the main liquid/gas interactions and to handle a polydisperse size distribution with a reduced computational cost has been developed in the framework of the open source code OpenFOAM (Jasak, 1996; Jasak et al., 2004). Considering the capabilities of the chosen approach for a general extension to scale resolved simulations, the solver is developed using a RANS approach.

The starting point of this work was the Eulerian solver derived from the Eulerian-Lagrangian Spray Atomization (ELSA) model (Borghi and Val-

let, 1999; Vallet et al., 2001): particular attention has been devoted to the modelling of the *turbulent liquid flux* term, that quantifies the effects of the relative velocity between liquid and gas on liquid distribution. First order closures for this term, based on the use of a standard gradient law of liquid volume fraction, were firstly analyzed in order to investigate their deficiencies in the study of atomization. Then, in order to extend the solver capabilities to the environment of current combustors, an innovative second order closure for turbulent liquid flux with a variable density turbulence treatment has been introduced. A detailed analysis of the resulting Quasi-Multiphase Eulerian (QME) solver capabilities is here presented exploiting a jet in crossflow test case in order to show the improvements that can be obtained in the description of liquid fuel distribution.

2. NUMERICAL APPROACH

ELSA model

The QME solver is based on the Eulerian solver derived from the Eulerian-Lagrangian Spray Atomization (ELSA) model. In the ELSA model, the two phase flow is studied as a single phase flow composed of two species with highly variable density. In the solution algorithm it is possible to distinguish an Eulerian framework, where the liquid distribution is calculated up to the generation of spherical droplets and a Lagrangian framework used to describe spray evolution. The reader interested in a detailed description of the ELSA formalism is addressed to the specific literature (Vallet et al., 2001; Lebas, 2007; Lebas et al., 2009; Beau, 2006; Demoulin et al., 2013).

In the Eulerian framework, the liquid phase evolution is determined by a liquid volume fraction (α_1) equation, while the breakup processes and the polydisperse spray distribution are accounted globally through the definition of the quantity of liquid/gas interface per unit of volume (Σ). It is worth noting that, in respect to droplet diameter, Σ is a very general quantity that can be defined ranging from a coherent film up to a diluted spray.

In this work, the two phases are assumed at constant density ρ so that turbulent fluctuations of mixture density ρ' are only due to volume fraction fluctuations following Equation 1.

$$\rho' = \rho_l \alpha_1' + \rho_g \left(1 - \alpha_1'\right) \tag{1}$$

This work considers the time-averaged governing equations of the Eulerian solver in ELSA which consist in conservation laws for momentum, gas/liquid interface density and volume fraction as reported in Equation 2. Continuity is enforced by means of pressure equation which is unmodified with respect to single phase flows thus it is not treated in this paper. RANS modelling was chosen in order to set up a robust and computationally cheap numerical tool. Nevertheless, proposed model have been implemented in OpenFOAM in a general way adaptable to both RANS and LES simply substituting τ_{ij}^t, that represents the viscous stress plus any additional term coming from turbulent fluctuations, with subgrid stresses in LES framework. Here, only RANS approach will be treated and considering a variable ϕ, its Reynolds average is denoted as $\bar{\phi}$ while its corresponding fluctuation as ϕ'.

$$\begin{cases} \dfrac{\partial \bar{\rho}\bar{U}_i}{\partial t} + \dfrac{\partial \bar{\rho}\bar{U}_j\bar{U}_i}{\partial x_j} = -\dfrac{\partial \bar{P}}{\partial x_i} + \bar{\rho}g_i + \dfrac{\partial \tau_{ij}^t}{\partial x_j} \\ \dfrac{\partial \bar{\Sigma}}{\partial t} + \dfrac{\partial \bar{U}_j\bar{\Sigma}}{\partial x_j} = \dfrac{\partial}{\partial x_j}\left(\bar{\Sigma}\left(\bar{U}_j - \bar{U}_{j|\Sigma}\right)\right) + \dfrac{\bar{\Sigma}}{\tau_t}\left(1 - \dfrac{\bar{\Sigma}}{\Sigma^*}\right) \\ \dfrac{\partial \bar{\alpha_1}}{\partial t} + \dfrac{\partial \bar{U_j}\bar{\alpha_1}}{\partial x_j} = \dfrac{\partial \bar{U_j}\bar{\alpha_1} - \overline{U_j\alpha_1}}{\partial x_j} = \dfrac{\partial(-R_{\alpha_1,j})}{\partial x_j} \end{cases} \tag{2}$$

No source term due to evaporation has been considered while concerning τ_{ij}^t such term has been supposed to be dominated by turbulent viscous stresses, exploiting a standard eddy-viscosity model for its closure. In this context, both two equations k-ϵ (Demoulin et al., 2007; Chassaing, 2001) and Reynolds Stress turbulence models (Launder et al., 1975) have been considered.

In system 2, the liquid volume fraction equation contains only one unclosed term, namely the *turbulent liquid flux* ($R_{\alpha_1,j} = \overline{u_j'\alpha_1'}$), that represents the transport of the liquid volume fraction induced by velocity fluctuations. This prevailing term describe liquid dispersion and normally, due to the high density ratio of two phase flow under consideration, this term may dominate momentum equation. Similarly, the first term on the RHS of the liquid/gas interface density equation, that accounts for the mean surface velocity, should be correctly modelled.

These terms are usually modelled with a *first order closure* by analogy with the Fick's law (Lebas et al., 2009; Lebas, 2007). In the next section, this kind of modelling will be discussed and its unrealiability for the description of lean injection systems flowfield will be shown. Then, an alternative and

innovative approach, specified as *second order closure*, will be introduced and validated in a experimental jet in crossflow test case.

First order closure

In this framework, it is possible to derive the following expression for turbulent liquid flux:

$$R_{\alpha_1,j} = -\frac{\nu_t}{Sc_t}\frac{\partial \bar{\alpha}_1}{\partial x_j} = -D_{gl,t}\frac{\partial \bar{\alpha}_1}{\partial x_j} \tag{3}$$

It is important to note that this approach is valid only in the absence of a mean slip velocity between liquid and gas and this can be justified considering that, if the phases are strictly immiscible, it is possible to derive the following exact definition for the turbulent liquid flux that shows the strong link between $R_{\alpha_1,j}$ and the local relative velocity $V_{rlg,j}$(Demoulin et al., 2007):

$$R_{\alpha_1,j} = \overline{u_j{}'\alpha_1{}'} = -\bar{\alpha}_1(\bar{U}_j - \bar{U}_{l,j}) = \bar{\alpha}_1(1-\bar{\alpha}_1)\bar{V}_{rlg,j} \tag{4}$$

It should be considered also that the local relative velocity, following the analysis developed by Deutsch and Simonin (1991) and in Simonin (2000), can be also re-arranged as:

$$\bar{V}_{rlg,j} = (\bar{U}_{l,j} - \bar{U}_{g,j} - \bar{V}_{D,j}) = (\bar{U}_{slg,j} - \bar{V}_{Dlg,j}) \tag{5}$$

This decomposition shows the two main components of the relative velocity in a particle two phase flow:

- an average relative velocity, here specified as $\bar{U}_{slg,j}$, between the particle and the surrounding flow in the promixity of the interface that is directly related to the drag force acting on the liquid
- a drift velocity ($\bar{V}_{Dlg,j}$) that is the conditional average of the fluid turbulent velocity fluctuation with respect to the particle distribution (Simonin, 2000).

Below, to avoid a too complex notation, the slip velocity $\bar{U}_{slg,j}$ will be specified as $\bar{U}_{s,j}$ and the drift as $\bar{U}_{D,j}$. The drift component accounts for the dispersion mechanism due to the particle transport by the fluid turbulent motion and it holds also in a mixture of two different species in a single phase flow. Indeed, it is related to a random agitation that promotes homogenization of phase concentration, leading to the generation of a mean average velocity. Hence, models developed in single phase flows can be exploited for its closure (Lebas et al., 2009). For example, considering the approach proposed by Bailly et al. (1997), where the turbulent flux of a scalar quantity in a single phase mixture is considered, the following classical gradient closure for drift flux is exploited:

$$V_{D,j} = \frac{D_{gl,t}}{\bar{\alpha}_1\left(1-\bar{\alpha}_1\right)}\frac{\partial \bar{\alpha}_1}{\partial x_j} \tag{6}$$

where $D_{gl,t}$ represents the liquid/gas turbulent dispersion coefficient.

Thus, if the spray dynamic relaxation time τ_p and the mean effective slip velocity $\bar{U}_{s,j}$ are negligible (i.e. in the case of droplets with low intertia) the turbulent liquid flux is only due to the drift velocity and Equation 3 can be exactly applied.

Under the same assumptions, the first term on the RHS of Σ can be modelled as a turbulent diffusion term (Lebas et al., 2009; Beau, 2006), neglecting the effects of the slip velocity on the liquid/gas interface density distribution.

$$R_{\Sigma,j} = \left(\bar{\Sigma}\left(\bar{U}_j - \bar{U}_{j|\Sigma}\right)\right) = \frac{\nu_t}{Sc_t}\frac{\partial \bar{\Sigma}}{\partial x_j} \tag{7}$$

It should be considered that some modifications to these single phase closure can be considered in order to include the effects of liquid inertia and liquid surface discontinuity (Simonin, 2000; Demoulin et al., 2007) but when the mean slip velocity is not negligible these formulations have to be deeply revised.

Considering the flowfield characteristics of lean combustor atomizer, the slip velocity can have a strong impact. This has been verified using the steady-state Eulerian-Lagrangian computations, available from (Andreini et al., 2014a, 2013), on the PERM injection system. An operating condition representative of IDLE (see Table 1) has been investigated and the computational domain corresponds to a 2D representation (1.5 degrees sector) of the tubular combustor, where swirler blades have been replaced by tangentially inclined air inlet boundaries at blade exit. From Lagrangian data it is possible to extract the spray evolution as in an Eulerian framerwork by averaging the properties of parcels cell by cell.

The chosen test condition is characterized by low pressure and by a locally high fuel-air ratio, with 20% of fuel that is injected through the pilot injec-

	Test point	Units
Gas inlet Temperature	613	K
Operating pressure	5	bar
m_{fp}/m_{ft}	20	%
Fuel Air Ratio	4.06	%
$\Delta P/P$	4.25	%

Table 1: Operating conditions of the investigated cases.

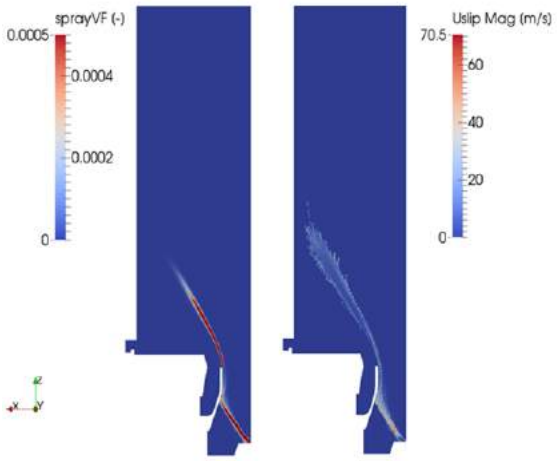

Figure 3: Evolution of slip velocity and liquid volume fraction on the symmetry plane.

tor and in Figure 3 is reported the obtained evolution of slip velocity and spray volume fraction. Because of the high value of Sauter Mean Diameter (SMD), due to low values of air inlet temperature, droplets fully evaporate far away from the injection location and particles injected through the pilot nozzle reach the prefilming surface. Near the pilot injector, due to the high inertia of liquid droplets, particles do not follow the gas stream, maintening a slip velocity up to the prefilming surface as high as 70 m/s. The importance of such velocity on the liquid distribution can be stressed also showing in Figure 4 the evolution of the ratio between the slip and the mixture velocity in the pilot region: locally U_s assumes values four time bigger than $\bar{U}$ and it gradually decreases due to the drag of the gas phase.

However, the relative importance of U_s in the pilot region with this geometrical configuration is very high and can not be neglected as it may have a strong effect on the liquid distribution. It is worth noting that the slip velocity should have a high impact also for injector configurations different from prefilming atomizers like the ones based on breakup of jets in crossflow (e.g. the TAPS atom-

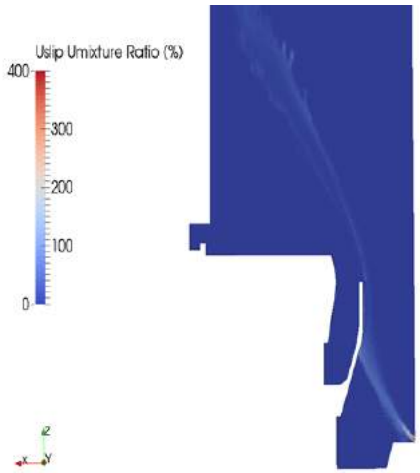

Figure 4: Zoom of the distribution of the ratio between the slip and the mixture velocity in the pilot region.

izer). Indeed, here the liquid mixing is completely controlled by discrete jets and, mainly in the region of jets impact, the slip velocity can be important. A detailed analysis of a jet in crossflow configuration is reported in Section 3.

Second order closure

In order to overcome the described issues in presence of a mean slip velocity, a second order model, in which each component of the turbulent liquid flux is individually analyzed, is proposed as a solution. A general formulation of the studied conservation equation may be the following one:

$$\frac{D\bar{\rho}\bar{R}_{\alpha_1,i}}{Dt} = \frac{\partial\bar{\rho}\overline{u_i'\alpha_1'}}{\partial t} + \frac{\partial\bar{\rho}\bar{U}_j\overline{u_i'\alpha_1'}}{\partial x_j} = \\ = \sum_{k=1}^{N}\Theta_k \tag{8}$$

Terms appearing on the RHS have to be properly closed and Θ_k stands for the N different physical phenomena that involve a production, destruction or transport of the turbulent liquid flux. For example, drag force, body forces, such as gravity, or any pressure gradient should be included in such term since they would lead to a different acceleration of each phase, because of the density ratio, and therefore to the generation of a relative velocity.

Starting from the review made by Beau (2006) on the possible approaches that can be used to close

Equation 8 in RANS context, a new transport equation for turbulent liquid flux is here proposed.

First of all, using Equation 5, the turbulent liquid flux is divided in a part due to the mean effective slip velocity (Υ_s) and one due to the drift (Φ_D) :

$$\begin{aligned} R_{\alpha_1,j} = \overline{u_j{}'\alpha_1{}'} &= \overline{u'_{jr}\alpha_1{}'} - \overline{u'_{jd}\alpha_1{}'} \\ &= \bar{\alpha}_1(1-\bar{\alpha}_1)(\bar{U}_{s,j} - \bar{V}_{D,j}) \\ &= \bar{\Upsilon}_{s,j} + \bar{\Phi}_{D,j} \end{aligned} \tag{9}$$

where:

$$\begin{cases} \bar{\Upsilon}_{s,j} = \bar{\alpha}_1(1-\bar{\alpha}_1)(\bar{U}_{l,j} - \bar{U}_{g,j}) \\ \bar{\Phi}_{D,j} = \bar{\alpha}_1(1-\bar{\alpha}_1)\bar{V}_{D,j} \end{cases} \tag{10}$$

As already discussed in the previous section, the term related to the drift flux is modelled with a gradient closure and hence the liquid volume fraction equation takes the following form:

$$\begin{aligned} \frac{\partial\bar{\alpha_1}}{\partial t} + \frac{\partial\bar{U}_j\bar{\alpha_1}}{\partial x_j} &= -\left(\frac{\partial}{\partial x_j}\left(\overline{u'_{jr}\alpha'_1}\right) + \frac{\partial}{\partial x_j}\left(\overline{u'_{jd}\alpha'_1}\right)\right) \\ &= -\left(\frac{\partial}{\partial x_j}\left(\bar{\Upsilon}_{s,j} + \bar{\Phi}_{d,j}\right)\right) \\ &= -\left(\frac{\partial}{\partial x_j}\left(\bar{\Upsilon}_{s,j}\right) - \frac{\partial}{\partial x_j}\left(\frac{\nu_t}{Sc_t}\frac{\partial\bar{\alpha_1}}{\partial x_j}\right)\right) \end{aligned} \tag{11}$$

A conservation equation for the component Υ_s is therefore necessary to close the problem. The unclosed formulation of such equation can be derived formally starting from Equation 8 and by applying Equation 10. Considering all the possible physical phenomena involved in Equation 8, such substitution leads to the following theoretical equation (Beau, 2006; Beau et al., 2005):

$$\begin{aligned} \frac{\partial\bar{\rho}\bar{\Upsilon}_{s,i}}{\partial t} + \frac{\partial\bar{\rho}\bar{U}_j\bar{\Upsilon}_{s,i}}{\partial x_j} = &\frac{\partial\bar{\rho}\overline{u'_iu'_j\alpha'_1}}{\partial x_j} + S_{gradU,i} + S_{grad\alpha1,i} + \\ &+ S_{evap} + S_{coll,i} + S_{drag,i} + \\ &+ S_{pressure,i} + S_{body\ forces,i} + \\ &+ S_{surf\ tension,i} + S_{viscous,i} \end{aligned} \tag{12}$$

The complement of such equation to recover the complete turbulent liquid flux can be exploited for the definition of a transport equation also for the drift flux. The unclosed terms in Equation 12 have to be addressed and here a phenomemological approach has been used focusing on slip effects. Remembering that for the operating conditions of gas turbine applications Weber and Reynolds numbers are usually very high, source terms due to surface tension ($S_{surftension}$) and viscous stresses ($S_{viscous}$) can be neglected. Furthermore, as highlighted by Beau (2006), the effects on the relative flux of droplets collision (S_{coll}) are negligible in comparison with the other physical phenomena and in order to simplify the mathematical formulation of the equation, the evaporation influence (S_{evap}) is overlooked. Source terms related to velocity gradients (S_{gradU}) and liquid volume fraction ($S_{grad\alpha1}$) are also neglected and are directly included into the drift part of turbulent liquid flux.

With these hypothesis an equation for Υ_s has been derived, where remaining source terms have been properly calculated starting from the momentum equation of liquid phase in an Eulerian framework as reported by Rusche (2002) and closing the triple correlation term with a gradient closure:

$$\begin{cases} S_{turb\ diffusion_i} = \left(\frac{\mu_t}{Sc_t}\frac{\partial\bar{\Upsilon}_{s,i}}{\partial x_j}\right) \\ S_{drag_i} = \bar{\rho}\frac{\bar{\Upsilon}_{s,i}}{\bar{\alpha_1}}\frac{\partial\bar{\alpha_1}}{\partial t} - \bar{\rho}\bar{\alpha_1}\frac{\partial\bar{U}_i}{\partial t} - \bar{\rho}\frac{n_d\bar{\Upsilon}_{s,i}}{(1-\bar{\alpha_1})\tau_p} \\ S_{pressure_i} = \bar{\rho}\bar{\alpha_1}(1-\bar{\alpha_1})\frac{1}{\rho_l}\frac{\partial\bar{P}}{\partial x_i} \\ S_{body\ forces_i} = \bar{\alpha_1}^2\frac{\rho_l}{\bar{\rho}}\left(1-\bar{\alpha_1}\frac{\rho_l}{\bar{\rho}}\right)(\rho_l-\rho_g)g_i \end{cases} \tag{13}$$

Leading to the following complete formulation:

$$\begin{aligned} &\frac{\partial\bar{\rho}\bar{\Upsilon}_{s,i}}{\partial t} + \frac{\partial\bar{\rho}\bar{U}_j\bar{\Upsilon}_{s,i}}{\partial x_j} = \frac{\partial}{\partial x_j}\left(\frac{\mu_t}{Sc_t}\frac{\partial\bar{\Upsilon}_{s,i}}{\partial x_j}\right) + \\ &+ \bar{\rho}\frac{\bar{\Upsilon}_{s,i}}{\bar{\alpha_1}}\frac{\partial\bar{\alpha_1}}{\partial t} - \bar{\rho}\bar{\alpha_1}\frac{\partial\bar{U}_i}{\partial t} - \bar{\rho}\frac{n_d\bar{\Upsilon}_{s,i}}{(1-\alpha_1)\tau_p} + \\ &+ \bar{\rho}\bar{\alpha_1}(1-\bar{\alpha_1})\frac{1}{\rho_l}\frac{\partial\bar{P}}{\partial x_i} + \\ &+ \bar{\alpha_1}^2\frac{\rho_l}{\bar{\rho}}\left(1-\bar{\alpha_1}\frac{\rho_l}{\bar{\rho}}\right)(\rho_l-\rho_g)g_i \end{aligned} \tag{14}$$

In the QME solver, this equation is coupled with the equation for liquid volume fraction and with the one for liquid/gas interface density. Indeed, as outlined in the previous section, the gradient closure is not sufficient even for this second equation if the slip velocity effects are important and therefore the turbulent liquid flux is used in order to recover a

more physical behaviour.

$$\begin{cases} \dfrac{\partial \bar{\alpha_1}}{\partial t} + \dfrac{\partial \bar{U}_j \bar{\alpha_1}}{\partial x_j} = -\left(\dfrac{\partial}{\partial x_j} \left(\bar{\Upsilon}_{s,j} + \dfrac{\nu_t}{Sc_t} \dfrac{\partial \bar{\alpha_1}}{\partial x_j} \right) \right) \\ \dfrac{\partial \bar{\Sigma}}{\partial t} + \dfrac{\partial \bar{U}_j \bar{\Sigma}}{\partial x_j} = -\dfrac{\partial}{\partial x_j} \left(\left(\dfrac{\bar{\Upsilon}_{s,j}}{\bar{\alpha_1}} + \dfrac{\nu_t}{Sc_t} \dfrac{\partial}{\partial x_j} \right) \bar{\Sigma} \right) + \\ \qquad + \dfrac{\bar{\Sigma}}{\tau_t} \left(1 - \dfrac{\bar{\Sigma}}{\Sigma^*} \right) \end{cases} \tag{15}$$

The proposed approach is similar to the *quasi-multiphase* method introduced by Beau (Beau, 2006; Beau et al., 2005), since the turbulent liquid flux may be used to evaluate both the liquid and the gas velocities through Equation 10. On the other side the two approaches differ since here a formulation in terms of turbulent volume flux has been adopted and the contribution from slip and drift velocities are accounted separately through the introduction of an innovative closure for $\Upsilon_{s,i}$ and the exploitation of a gradient closure for the drift component. This is surely the major modelling hypothesis since in this way all physical phenomena are reduced to diffusion mechanisms except for the ones directly related to slip equation. On the other hand, the major advantage of this method is the set-up of a robust and reliable solver from an industrial perspective able to include the most important phenomena acting on a dispersed phase.

Moreover, even if the proposed method is mathematically equivalent to a classical multiphase Eulerian-Eulerian solver, since a complete kinematic description is achievable using the information obtained from the slip flux equation, it is important to underline that in a quasi-multiphase environment the two-phase flow is studied as a single phase flow, thus it is possible to exploit models developed for the monophase mixtures (i.e. combustion model). Furthermore, the QME solver, using a velocity of the mixture and the information available from the liquid/gas interface density equation, avoids the selection about which phase should be considered as discrete or continuous and allows to describe all ranges from continuous phase to dilute spray with the same mathematical approach. On the other side, in comparison with the Eulerian *sectional* approaches it is possible to characterize, through the liquid/gas interface density equation, a polydisperse size spray without significantly increasing the computational effort.

In Table 2 the complete system of equations implemented in the QME solver is briefly reported.

Momentum equation:

$$\frac{\partial \bar{\rho} \bar{U}_i}{\partial t} + \frac{\partial \bar{\rho} \bar{U}_j \bar{U}_i}{\partial x_j} = -\frac{\partial \bar{P}}{\partial x_i} + \bar{\rho} g_i + \frac{\partial \tau_{ij}^t}{\partial x_j}$$

Liquid volume fraction equation:

$$\frac{\partial \bar{\alpha_1}}{\partial t} + \frac{\partial \bar{U}_j \bar{\alpha_1}}{\partial x_j} = -\left(\frac{\partial}{\partial x_j} \left(\bar{\Upsilon}_{s,j} \right) - \frac{\partial}{\partial x_j} \left(\frac{\nu_t}{Sc_t} \frac{\partial \bar{\alpha_1}}{\partial x_j} \right) \right)$$

Liquid gas interface density equation:

$$\frac{\partial \bar{\Sigma}}{\partial t} + \frac{\partial \bar{U}_j \bar{\Sigma}}{\partial x_j} =$$
$$-\frac{\partial}{\partial x_j} \left(\frac{\bar{\Upsilon}_{s,j}}{\bar{\alpha_1}} \bar{\Sigma} \right) + \frac{\partial}{\partial x_j} \left(\frac{\nu_t}{Sc_t} \frac{\partial}{\partial x_j} \bar{\Sigma} \right) + \frac{\bar{\Sigma}}{\tau_t} \left(1 - \frac{\bar{\Sigma}}{\Sigma^*} \right)$$

Turbulent liquid flux equation:

$$\frac{\partial \bar{\rho} \bar{\Upsilon}_{s,i}}{\partial t} + \frac{\partial \bar{\rho} \bar{U}_j \bar{\Upsilon}_{s,i}}{\partial x_j} =$$
$$+\frac{\partial}{\partial x_j} \left(\frac{\mu_t}{Sc_t} \frac{\partial \bar{\rho} \bar{\Upsilon}_{s,i}}{\partial x_j} \right) + \bar{\rho} \frac{\bar{\Upsilon}_{s,i}}{\bar{\alpha_1}} \frac{\partial \bar{\alpha_1}}{\partial t} +$$
$$-\bar{\rho} \bar{\alpha_1} \frac{\partial \bar{U}_i}{\partial t} - \bar{\rho} \frac{n_d \bar{\Upsilon}_{s,i}}{(1-\alpha_1)\tau_p} + \bar{\rho} \bar{\alpha_1} (1 - \bar{\alpha_1}) \frac{1}{\rho_l} \frac{\partial \bar{P}}{\partial x_i} + \bar{\alpha_1}^2 \frac{\rho_l}{\bar{\rho}} \left(1 - \bar{\alpha_1} \frac{\rho_l}{\bar{\rho}} \right) (\rho_l - \rho_g) g_i$$

Table 2: Summary of the equations implemented in the QME solver in OpenFOAM.

3. VALIDATION OF THE QME SOLVER

Preliminary validation

To firstly clarify the improvements that can be obtained using the proposed QME solver and to underline once again the limitations of first order closure, a preliminary test case, where an homogeneous cloud of droplet with an average velocity ΔU is moving into a quiescent medium (see Figure 5), has been considered.

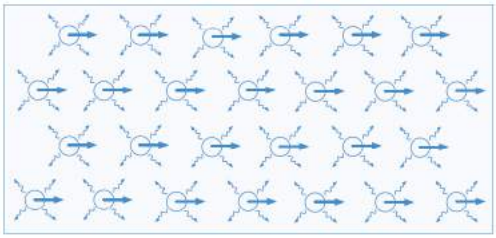

Figure 5: Homogenous cloud of droplet moving into a quiescent medium (taken from Lebas (2007)).

In such condition, the model proposed in Equation 3 (i.e. first order closure) entails a paradox with Equation 4 because, since the distribution of droplets is uniform in space, a zero value of turbulent liquid flux is calculated from the gradient closure whereas a non zero value is predicted from its definition. This is a key point since the turbulent liquid flux contains turbulent diffusion phenomena related to turbulent random fluctuations but also the mean slip velocity between gas and liquid phases according to the exact Equation 4. After

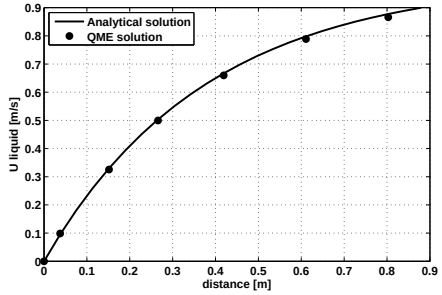

Figure 6: Comparison of analytical and QME results for 1D test case

a certain time (i.e. the particle relaxation time), because of the drag force, the slip velocity between the two phases becomes zero but during this transition the first order closure is not adequate and cannot be applied. On the other hand, the QME approach is able to properly depict this situation since the slip velocity is taken into account through Equation 14.

Hence, considering a 1D-test case, representative for Figure 5, where a liquid droplet, with an initial velocity, is inserted in a gas flow with a non zero relative velocity, it has been possible to make a comparison between the liquid velocity obtained through equations presented in Table 2 and the one that can be analitycally calculated from the definition of the dynamic relaxation time (τ_p) (for further details about its mathematical definition and derivation see (Giusti, 2013)):

$$U_{liquid} = U_{gas}\left(1 - e^{\left(-\frac{t}{\tau_p}\right)}\right) \qquad (16)$$

Figure 6 shows that the agreement between the numerical and the analytical solution is excellent, leading to the preliminary conclusion that the solver is able to properly reproduce the main interactions of a two phase flow subjected to a slip velocity where a first order closure cannot be exploited. This simple test case demonstrate also that is mandatory, for turbulent liquid flux approaches to complete any closure by a dedicated two phase flow model able to introduce the slip velocity between the gas and the liquid.

Obviously, such theoretical validation is not satisfactory for completely testing the capabilities of the QME solver, hence in the next section a jet in crossflow test case have been used for the assessment of the developed solver.

Jet in crossflow test case

The experimental measurements realized by Brown and McDonell (2006) on a jet in crossflow configuration was chosen for the validation of the QME approach because of its geometrical simplicity and the availability of accurate measurements for a wide range of operating conditions. Indeed, such test guarantees high slip velocity in the region of interaction between the jet and the crossflow and a full range of liquid volume fraction making it suitable for a simultaneous validation of different solver aspects. Furthermore, its engineering relevance, due to the high energy transfer between the phases, is proved by many applications in fuel atomization, lubrication and cooling considering aeroengines devices.

Figure 7 shows a schematic representation of the experimental set up. The injector consists of a long pipe of 7.49 mm diameter, followed by a 118deg angled taper section and by a short pipe of diameter d_{jet} with $L/d_{jet} = 4$, whose exit is mounted flush with the lower channel wall. Jet characteristics were measured for several values of d_{jet} and here the experimental results with d_{jet} =1.30 mm are used. The experimental tests have been real-

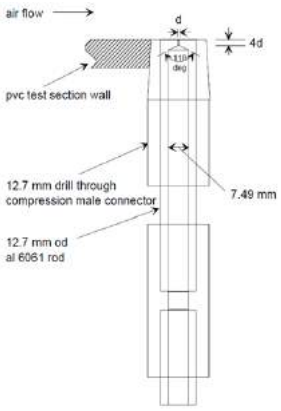

Figure 7: Main characteristics of the considered jet in crossflow test case (Brown and McDonell, 2006).

ized using a jet of water into a crossflow of air and the jet penetration has been evaluated for several values of the momentum flux ratio ($q = \frac{\rho_j {U_j}^2}{\rho_c {U_c}^2}$) and of the crossflow Weber number ($We_c = \frac{\rho_c {U_c}^2 d_{jet}}{\sigma}$). Using a high speed camera, the jet penetration has been determined measuring, for each column of pixels in the crossflow direction, the rows containing the minimum and maximum volume fraction values. Hence, for a discrete set of constant locations, starting from its corresponding maximum value, the

Quantity	Value
Momentum ratio	6.6
Crossflow Weber Number	330
Jet Weber Number	2178
Crossflow Reynolds number	5.7e+05
Jet Reynolds Number	1.4e+04

Table 3: Operating conditions of the chosen test point.

outer edge was determined when the pixel intensity had dropped to 50 % of the maximum local value. Then, starting from the correlations proposed by Wu et al. (1997) and Stenzler et al. (2006), values of prefactor and exponent coefficients have been modified in order to correctly predict the jet penetration with this experimental setup, leading to the following correlations (Brown and McDonell, 2006):

$$\begin{cases} \dfrac{y}{d_{jet}} = 1.50 \left(\dfrac{x}{d_{jet}}\right)^{0.35} q^{0.47} & \text{(17a)} \\ \dfrac{y}{d_{jet}} = 2.45 \left(\dfrac{x}{d_{jet}}\right)^{0.33} \dfrac{q^{0.50}}{We_c^{0.061}} \left(\dfrac{\mu_l}{\mu_{H_2O}}\right)^{-0.027} & \text{(17b)} \end{cases}$$

As reported in (Brown and McDonell, 2006; Herrmann, 2010), the Equation 17b, including the crossflow Weber number, is more suitable for the outer edge prediction and it will be used as reference in this work. The other one will be used only for qualitative comparisons.

It should be also considered that both these relations can be used up to a maximum dimensionless axial distance from injector exit (using d_{jet} as reference length) of X=10 since the experimental measurements have been realized only in the region just downstream the injection point (Brown and McDonell, 2006; Herrmann et al., 2011).

In the present study, the test characterized by the operating conditions reported in Table 3 has been considered.

Computational setup

Figure 8 shows the computational domain and the chosen boundary conditions employed in the presented simulations. The domain dimensions (-$25d_{jet}$...$50d_{jet}$ × -$23d_{jet}$...$25d_{jet}$ × -$10d_{jet}$...$10d_{jet}$), similar to the one used in (Herrmann et al., 2011), are smaller than the channel used in the experiments (-$77d_{jet}$...$127d_{jet}$ × $0d_{jet}$...$54d_{jet}$ × -$27d_{jet}$...$27d_{jet}$), but as highlighted in (Herrmann et al., 2011; Herrmann, 2010) the reduced dimensions can be safely considered not affecting the obtained results. The liquid pipe is included in the computational domain in order to correctly predict the exit flowfield required for a proper modelling of the interaction between the jet and the crossflow.

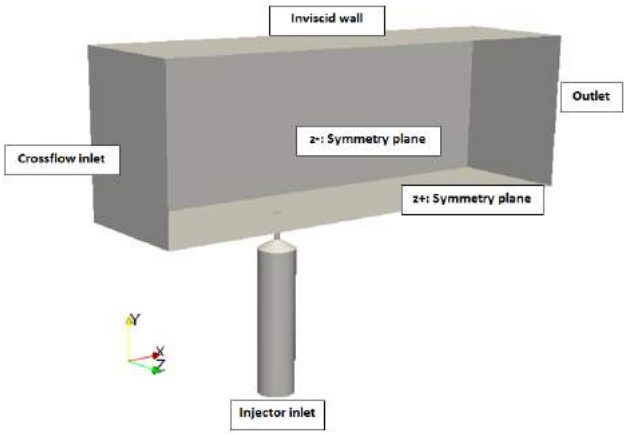

Figure 8: Computational domain and boundary conditions used in the simulations.

Applied boundary conditions follow a classical scheme for steady incompressible flows with an uniform velocity prescribed at both inlet boundaries and static pressure assigned on the outlet. The lateral surfaces are considered as symmetry planes, whereas the upper surface is modelled like an inviscid wall. The injector surfaces as well as the lower channel boundary are modelled with a no-slip condition and in this work both a standard wall-function and Launder and Sharma (1974) low-Reynolds treatment has been employed for boundary layer modelling and will be compared in the next section. A zero gradient condition has been imposed at wall both for the liquid volume fraction and for the liquid/gas interface density, while the turbulent liquid flux is imposed null as all the other convective fluxes.

Both the turbulent liquid flux and the liquid/gas interface density are characterized by boundary values equal to zero for the liquid and crossflow inlet as only one phase is present on those surfaces.

Computations were carried out on the hybrid unstructured grid depicted in Figure 9, created using ICEM-CFD. Tetrahedral elements fill up the crossflow region while the near wall zone is made of prismatic elements to maximise near wall orthogonality on the viscous surfaces. Four meshes, with different levels of refinemements in the region where the

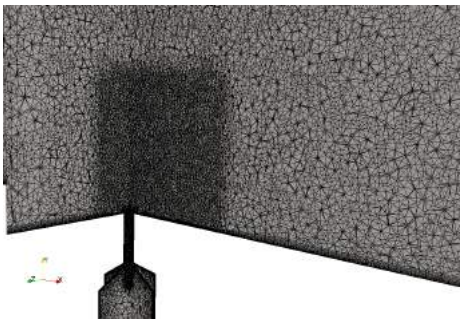

Figure 9: Computational domain for the jet in crossflow test case.

Mesh	Mesh elements	Min Element size
A	$1.9e^6$	0.2 mm
B	$3.2e^6$	0.15 mm
C	$6.0e^6$	0.1 mm
D	$2.0e^6$	0.2 mm

Table 4: Mesh sensitivity parameters.

two jets collide (see Table 4), have been considered during the study, in order to assess the dependency of results on the chosen computational domain. It should be pointed out that mesh D, with similar elements number of mesh A, is characterized by a local refinement in the boundary layer to guarantee $y+$ values consistent with a low-Reynolds wall treatment and to make a comparison with standard wall-function strategy adopted for the other computational domains.

The solver follows a classical SIMPLE loop to solve the pressure-velocity coupling and both convective and diffusive flux are discretized following bounded second order schemes to maximize the accuracy with a symmetric VanLeer limiter on liquid volume fraction equation in order to bound it between 0 and 1.

As suggested in (Herrmann et al., 2011), a density ratio ($R = \frac{\rho_{jet}}{\rho_c}$) lower than the experimental one has been firstly imposed (R=10) and, in order to maintain the characteristic numbers shown in Table 3, the velocity ratio has been properly modified. A sensitivity analysis both on computational domain and on turbulence modelling is reported at the beginning of the next section using a first order closure for turbulent liquid flux in order to define the most suitable and robust numerical setup that will be used to show the enhancement achievable with the QME in such test conditions. Then, as it will be shown in the final part of the paper, results for the experimental density ratio (R=1000) are also considered in order to validate the solver in a high density ratio environment typical of fuel injector in actual lean combustors.

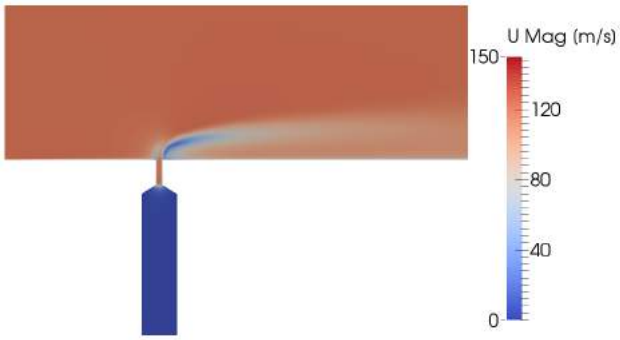

Figure 10: Mixture velocity distribution on the symmetry plane with first order closure.

R=10 test case

Figure 10 shows the mixture velocity distribution on the symmetry plane obtained exploiting Equation 3 for turbulent liquid flux: due to its higher momentum, the liquid jet is seen as an obstacle by the gas flow leading to the formation of a recirculation zone extended up to an axial distance of X=2 from the injector exit. The resulting blockage leads to an acceleration of the crossflow achieving a maximum local velocity around $U_{max} = 140m/s$. The reader interested in a more detailed description of the flow field characteristics in a jet in crossflow case is adressed to reference (Smith and Mungal, 1998).

The mixture velocity field is not significantly affected by the tested mesh resolution as can be appreciated in Figure 12 where profiles of mixture axial velocity along the non-dimensional Y direction, with d_{jet} used as reference length, are compared for planes shown in Figure 11. All these comparisons have been realized using a $\kappa - \epsilon$ model coupled with a wall-function treatment.

As already pointed out, a recirculation region, that disappears at the second axial position, can be identified and the radial extension of such bubble is nearly the same with the different mesh resolutions. The presence of the liquid jet, that is characterized by a lower axial velocity, can be clearly appreciated around Y=2 and it should be underlined that, moving downstream, using a first order closure, the decrease of the slip velocity between the two phases is

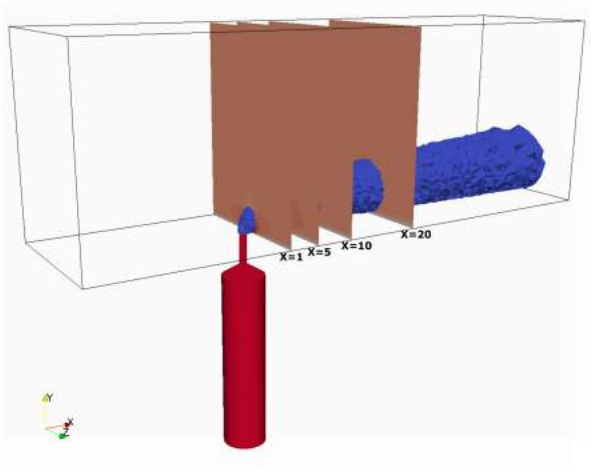

Figure 11: Position of planes considered for sensitivity analysis.

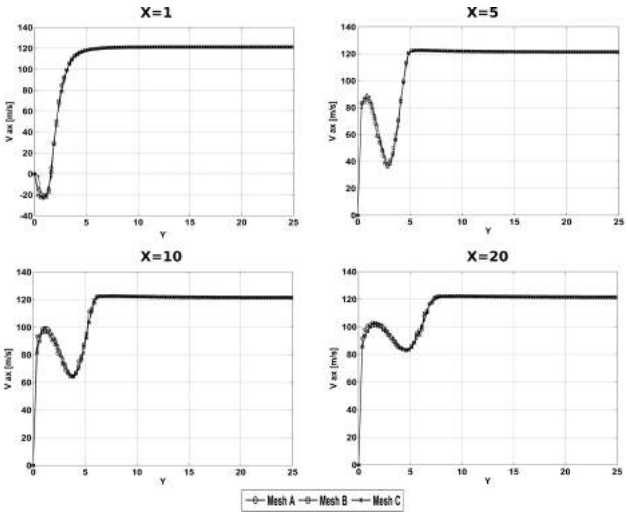

Figure 12: Axial velocity profiles along Y direction at different axial positions.

wrongly caused only by the diffusion predicted by the turbulence model. No appreciable differences between the tested meshes in terms of mixture velocity have been again determined also for planes far from the injection. Similarly, the liquid volume fraction distributions, that have not been reported here for the sake of clarity, are similar between the three meshes. Hence, in the light of these results and to minimize the computational effort, in the following results obtained with mesh A will be considered.

Directly related to the velocity field, the jet trajectory and the turbulent liquid breakup has been analyzed with a direct comparison with the experimental correlations. As reported in (Herrmann, 2010), the definition of the penetration in a jet in crossflow configuration is not straightforward. The simplest approach could be to define the jet trajectory as the maximum height from the wall where volume fraction is above a certain threshold value. However, a strong dependency on the constant α_1 value chosen in order to identify the windward edge trajectory has been observed. In (Herrmann et al., 2011), where a Refined Level Set Grid method (*RLSG*) is employed to directly track the motion of the liquid/gas interface in the same test case, an alternative approach is implemented with an average on the Heaviside transform of the level set scalar. In this manner, it is possible to define a scalar, consisting in a mean liquid volume fraction, that describes the probability of finding liquid at a given location. The resulting probability isolines

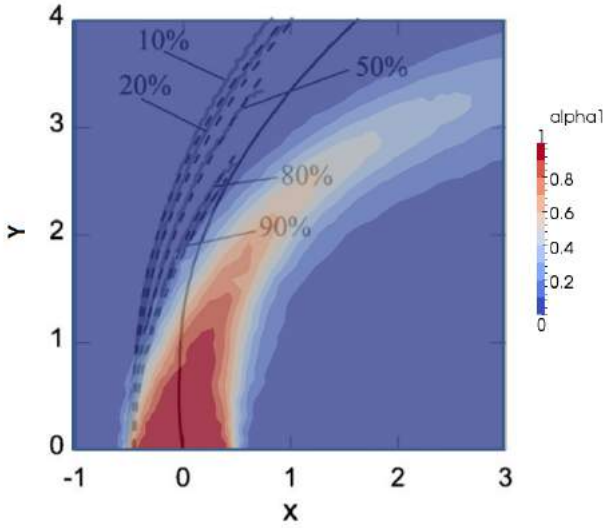

Figure 13: Impact of the chosen threshold value for α_1 value on windward edge trajectory (Herrmann, 2010) with first order liquid volume fraction results.

(Herrmann et al., 2011; Herrmann, 2010), reported as function of non dimensional coordinates (X,Y) are shown in Figure 13 superposed to current CFD first order volume fraction predictions. Such curves are superposed to the liquid volume fraction field obtained with the first order closure and scaled in order to obtain a ten levels contour. From a qualitative point of view it can be pointed out that a strong spread in the outer edge prediction is determined depending on the chosen threshold value for α_1; this highlights a potential weakness in the

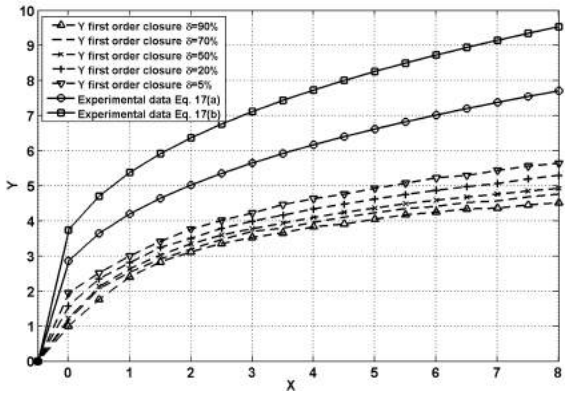

Figure 14: Comparison of the penetration obtained with the first order closure for different δ values against experimental data.

definition of jet penetration, even if a strong underprediction can be already verified.

In order to quantitatively understand such error, the comparison with the experimental correlations has been realized exploiting the method suggested by Brown and McDonell (2006), thus calculating the windward edge trajectory as the locus of points where, for each line in Y direction, the liquid volume fraction decrease below a specified δ% of the local maximum. Even if in the experimental paper a value of δ=50% is specified, a sensitivity to the chosen δ was performed on the results obtained with the first order closure for the turbulent liquid flux as shown in Figure 14 against experimental correlations (see Equation 17). As in steady-state approaches the centerline values of coherent jets are usually overestimated (Acharya et al., 2012), it is reasonable to choose a lower value of δ compared to experiments. The curves obtained for 5 different values of δ ranging from 5% to 90% reveal a moderate influence to such parameter with total spread limited to 1 d_{jet} in the investigated range. Hence, for the proposed test case it has been preferred to define the windward jet edge following δ = 5% curve.

Despite the reduced value of δ compared to the experiments, for the first order closure the penetration is strongly underestimated obtaining a maximum deviation from Equation 17b above 40% directly at the jet injection. Moreover, defining an effective deviation ξ between numerical and experimental data in the investigated range ($0.5 < X < 8$) as the root mean square of the error between the two sets of values, a value of ξ=39% has been obtained.

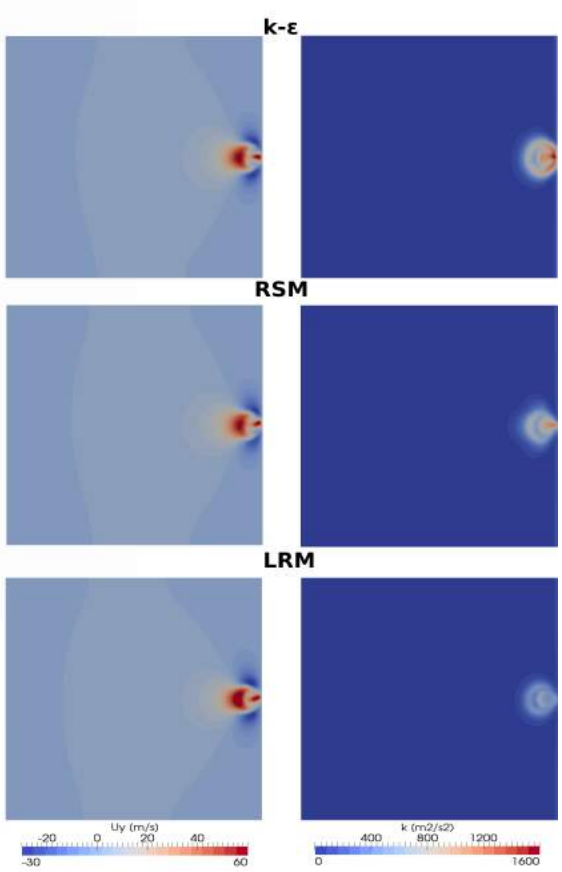

Figure 15: Comparison of the velocity and turbulent kinetic energy obtained with the first order closure combined with three turbulent models from top to bottom: k-ϵ, Reynolds Stress Model and Low Reynolds Model.

Furthermore, considering that, based on Equation 3, the liquid volume fraction field, with a first order closure, is completely determined by the turbulent viscosity, a sensitivity analysis has been realized both on turbulence model and wall treatment. Reynolds stress model (RSM) proposed by Launder et al. (1975) and Launder and Sharma (1974) low Reynolds (LRM) wall treatment have been considered in this context. Such models have been chosen to explore possible effects of free-stream and near wall turbulence anisotropy respectively. It is known in fact that simulations of a jet-in-crossflow may be strongly affected by the choice of the turbulence model, especially in the near wall region, also for single phase flows (Bianchini et al., 2013). In Figure 15 the Y-velocity component and turbulent kinetic energy contours obtained with considered turbulence models are reported for plane X=1:

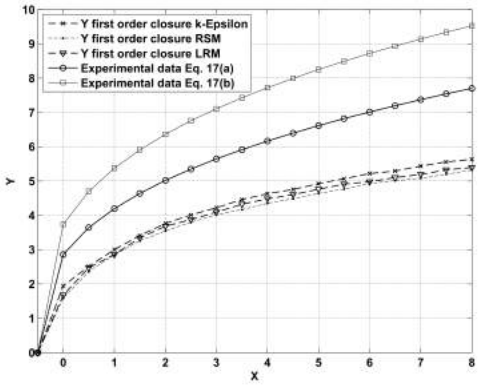

Figure 16: Comparison of the penetration obtained with the first order closure combined with several models for turbulent quantities.

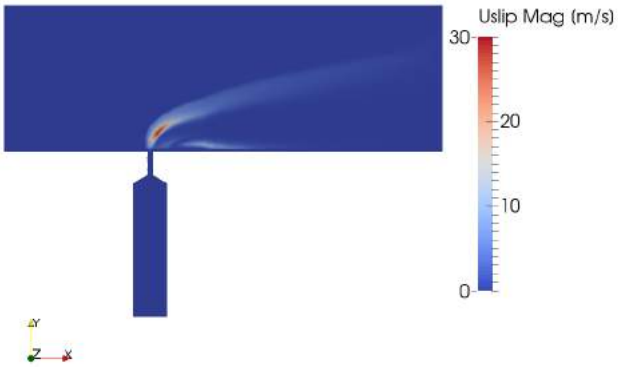

(a) .

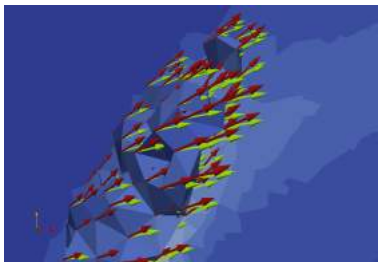

(b) .

Figure 17: Slip velocity distribution on the symmetry plane obtained using the QME solver (a) and a vectorial comparison between liquid (red) and gas (green) velocity in the impact region (b).

the blockage, determined by the liquid jet, is very similar in the three cases and only with LRM a higher extension of kidney vortex of around 10 % is predicted. On the other hand, levels of turbulent kinetic energy are very different mainly in the near wall region where the two jets clash and it is worth noting that LRM generally gives lower values than the other two models. Such findings are in agreeement with numerical results reported in (Hoda et al., 2000).

In terms of penetration, the comparison is shown in Figure 16 and it should be pointed out that the same penetration is predicted independently on the chosen turbulence model. Hence, in the context of first order closure approaches, in RANS context, the liquid jet penetration is not mainly affected by the chosen turbulence model. Indeed, turbulent liquid-gas flows demonstrate particular features that cannot be handled with standard turbulent models originally developed for single phase flows. This finding is in agreement with previous study in this field (Demoulin et al., 2007). The key characteristic of the liquid jet injected in crossflow is the slip velocity that experience any droplet before to relax to the gas velocity. This is the purpose of the QME solver (see Table 2) to appreciate not only the mixture velocity, but even separately liquid and gas velocity. The slip velocity, shown in Figure 17, is mainly generated where the two jets collide because of the high pressure gradient, while more downstream the reduction of the relative velocity is mainly led by the drag term. In the same figure, a vectorial comparison is also reported between the velocity of the two phases in the region where the slip velocity takes its maximum value in order to underline the effects of the turbulent liquid flux on the flowfield.

The predicted relative velocity sensibly modifies the liquid distribution into the domain, as shown in Figure 18 where a vector plot of the slip velocity on the iso-surface identified by $\alpha_1 = 0.5$ is reported. Jet penetration is much better predicted with respect to the first order closure as shown in the quantitative comparison with experimental correlations in Figure 19. In this case, the discrepancy with the experimental results is reduced both in terms of maximum value at X$\simeq$0.0 and effective deviation which decreases down to ξ=28%.

Thus, the impact of second order closure on liquid distribution at the chosen operating conditions is significant and positively affects the agreement with experimental evidences, even if a quite large underprediction is still found. The obtained underprediction can be justified considering that the effects of the velocity and liquid volume fraction gradient

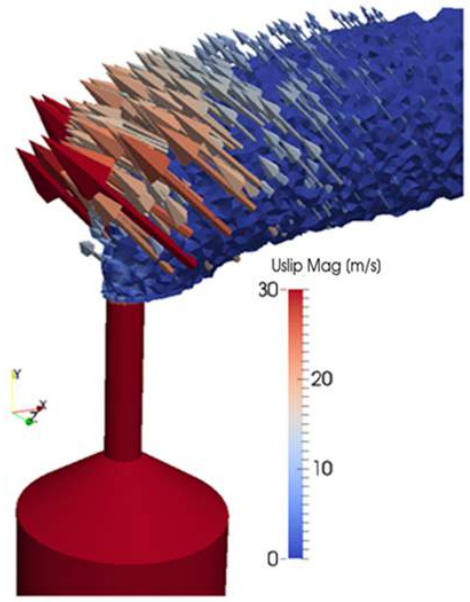

Figure 18: Vectorial representation of the slip velocity on liquid volume fraction iso-surface.

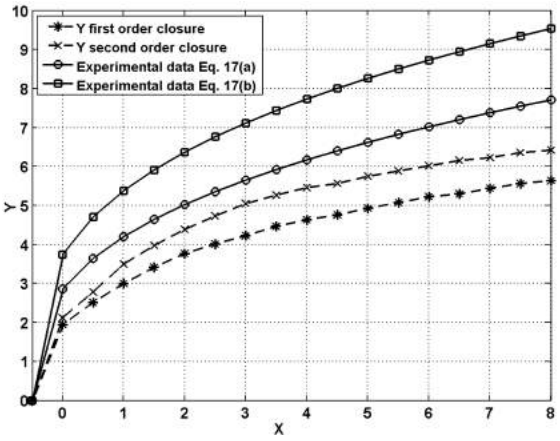

Figure 19: Comparison of the penetration predicted by the QME solver against first order closure and experimental results.

on the turbulent liquid flux distribution have been neglected. These sources of relative flux should be negligible at the experimental operating conditions but may have a higher impact in this case due to the reduced density ratio. Moreover, the high error in the penetration prediction, determined for small values of X, may be due to the employed turbulence model in a case where the turbulent field contribution is essential(Herrmann et al., 2011; Herrmann, 2010). Further developments are required on this point exploiting an extension of the solver to LES

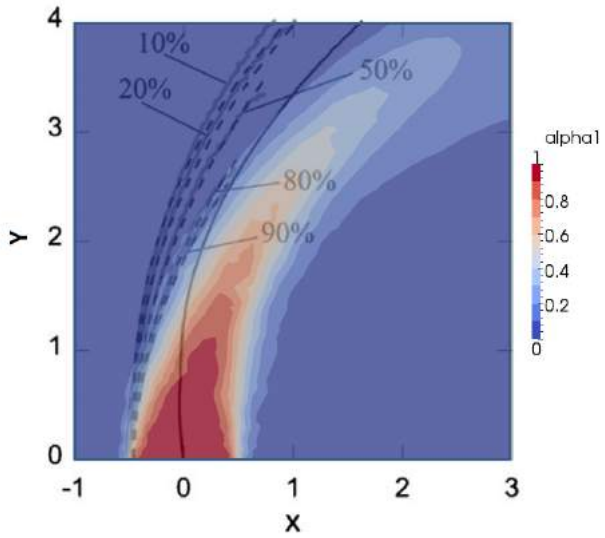

Figure 20: Comparison of the probability isolines in (Herrmann, 2010) with the liquid volume fraction field obtained with the second order closure.

formalism.

Figure 20 shows a qualitative comparison between the liquid volume fraction field, obtained using the QME solver, and the previously introduced probability isolines obtained in Herrmann (2010): even though the jet trajectory is still underpredicted in large part of the analyzed region compared to (Herrmann et al., 2011), the improvements obtained with the developed closure with respect to the original modelling reported in Figure 13 are considerable especially for X$\geq$1/2.

Furthermore, it is possible to verify the solver capability in predicting a polydisperse spray showing the distribution of the Sauter mean diameter, determined as $D_{32} = \frac{6\alpha_1}{\Sigma}$, compared with the one obtained with the first order closure on the symmetry plane as depicted in Figure 21. The behaviour in the two cases is quite similar, since the diameter takes its highest value at the injector exit decreasing downstream because of the turbulent breakup. However, it can be pointed out that, in Figure 21b, lower values of droplets diameter are predicted. Indeed, the introduction of the turbulent liquid flux into Σ equation introduces the effects of relative velocity on liquid breakup and the existence of a slip velocity physically brings to a more violent atomization process (Dumouchel, 2008).

This section has shown the behaviour of QME approach in a reduced density ratio environment and the obtained results have been compared with

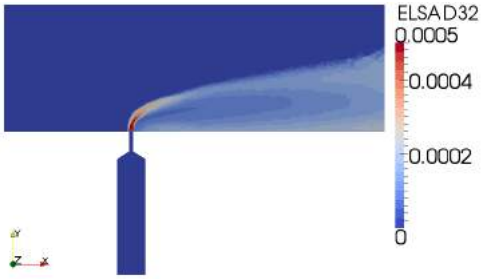

(a)

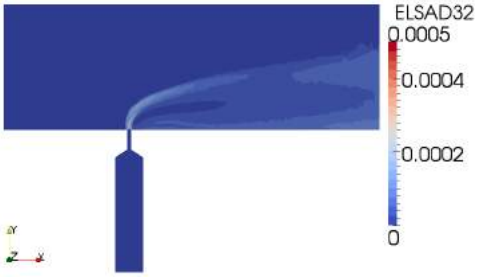

(b)

Figure 21: Characteristic droplet diameter evolution on the symmetry plane with first order (a) and second order (b) closure.

(a)

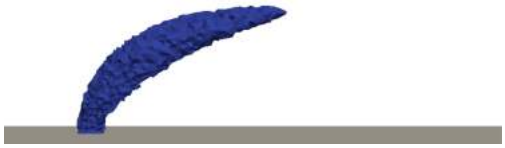

(b)

Figure 22: Liquid volume fraction isosurfaces (α_1=0.05) obtained at R=10 (a) and R=1000 (b).

RLSG data reported in (Herrmann, 2010). In the next section the experimental density ratio results will be discussed.

R=1000 test case

The increase of the density ratio leads to a different behaviour of the jet as shown in Figure 22 where

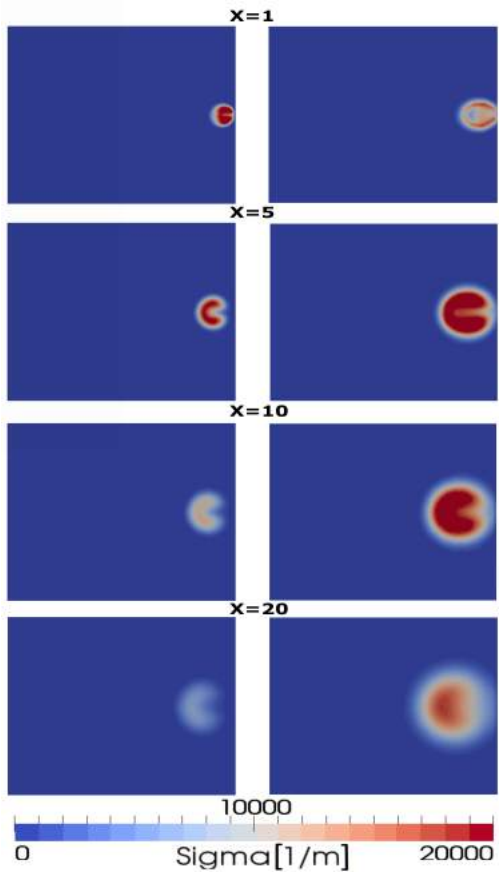

Figure 23: Liquid/gas interface density distributions at different axial distances with R=10 (left) and R=1000 (right) .

liquid volume fraction isosurfaces for α_1 =0.05 obtained with the first order closure at the two tested density ratio are compared. As explained also in (Herrmann, 2010), the jet is less bent and extended in the crossflow direction in R=1000 test case with a strong enhancement of its penetration. Furthermore, even if the liquid core appears initially more compact, the resulting spray shows a higher spreading in the jet transverse direction as depicted in Figure 23 where front views of liquid/gas interface density distributions at several axial distances are compared. It should be pointed out that near the injector lower values of Σ are predicted in the higher density ratio case since the jet is less prone to breakup in droplet, while with R=10 a strong and violent deformation of the circular jet cross section is immediately determined. However, at higher axial distances, a strong production of Σ, due to the growth of higher surface instabilities oc-

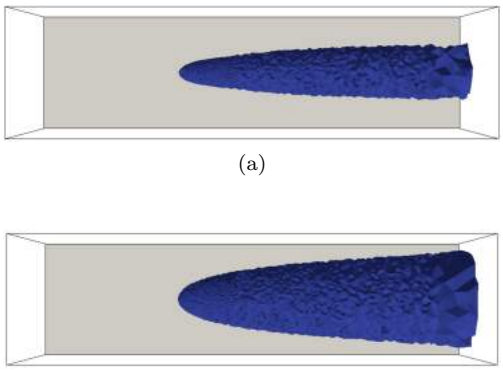

(a)

(b)

Figure 24: Liquid/gas interface density isosurfaces (Σ =30000) obtained at R=10 (a) and R=1000 (b).

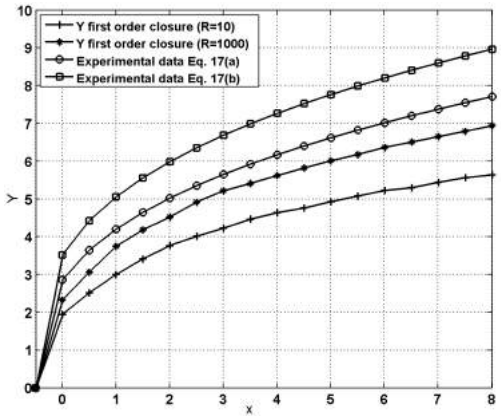

Figure 25: Comparison of the penetration obtained with a first order turbulent liquid flux closure with experimental results.

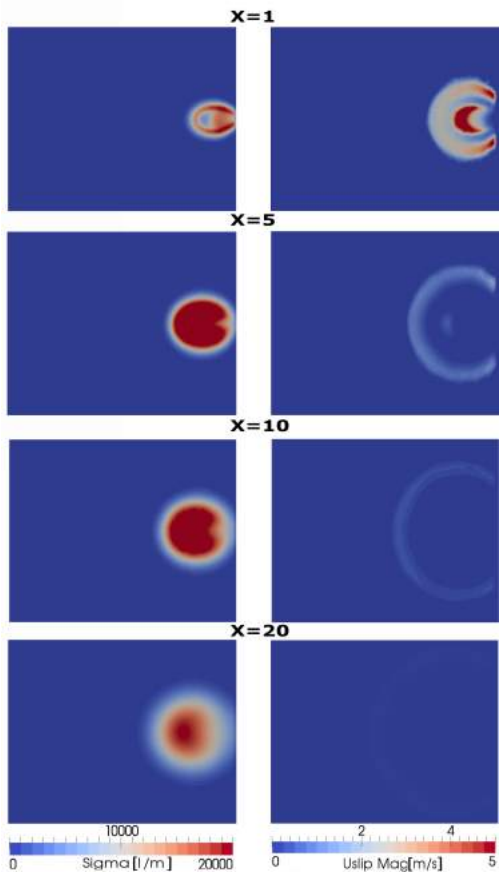

Figure 26: Liquid/gas interface density and slip velocity distribution at different axial distances.

curs, leading to the generation of a spray with a broad range of drop sizes that tends to follow the gas phase and to determine the jet spreading. This is also confirmed in Figure 24 where top views of liquid/gas interface density isosurfaces for Σ =30000 with the two tested density ratio are compared in order to highlight the higher spreading predicted with R=1000. It should be underlined that these findings are qualitatively in agreement with numerical results reported in Herrmann (2010) as well as experimental data shown in (Bellofiore et al., 2007; Elshamy and Jeng, 2005).

On a quantitave point of view, in Figure 25 the penetration obtained at the two tested density ratio with first order closure is compared with the experimental results (Brown and McDonell, 2006). A strong underprediction is still obtained for the liquid penetration and, maintaining the previously defined methodology, the effective deviation in respect to Equation 17b decreases only down to ξ=25%.

As in the previous section, the QME solver leads again to a more reliable description of the liquid distribution since the slip velocity increases the jet penetration and, considering the previously highlighted underprediction, this leads to a more physical prediction of the jet penetration in the gas crossflow. In Figure 26 the evolution of the liquid/gas interface density and of the slip velocity obtained with the second order closure in the same planes is reported. With respect to Figure 23, the presence of a slip velocity, that takes its peak value in the first trasversal section where the two jets collide, immediately tends to promote the growth of surface instabilities that leads to a quick atomization in the proximity of the jet exit. The core of the spray, characterized by high values of Σ and low SMD, due to the drag force, follows the gas phase and spreads out in the transverse direction while the

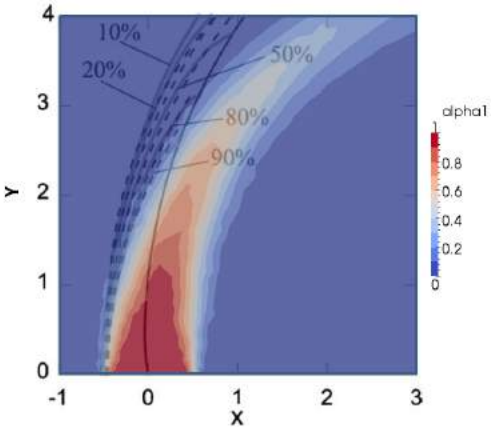

(a)

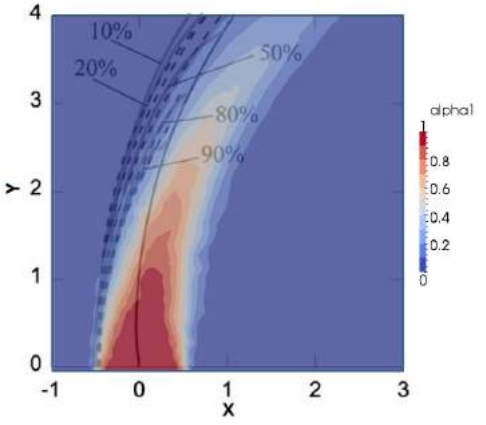

(b)

Figure 27: Comparison of the probability isolines in (Herrmann, 2010) for R=100 with the liquid volume fraction field obtained with first order (a) and second order (b) closure with R=1000.

outer part maintain a non zero slip velocity. Going downstream, such velocity between the two phases disappears and indeed, at $X = 20$, the liquid/gas interface distribution determined with second order closure is similar to the one already shown in Figure 23. This behaviour is again in agreement with experimental findings reported in (Lubarsky et al., 2012; Freitag and Hassa, 2008) and it is also representative for results obtained in previous numerical works as stated by the qualitative comparison, reported in Figure 27, between the liquid penetration achieved with the QME solver and probability isolines obtained for R=100 in (Herrmann, 2010). Even if the chosen density ratio is different, the relative enhancement with respect to Figure 27a is evident and it is due to the slip turbulent liquid

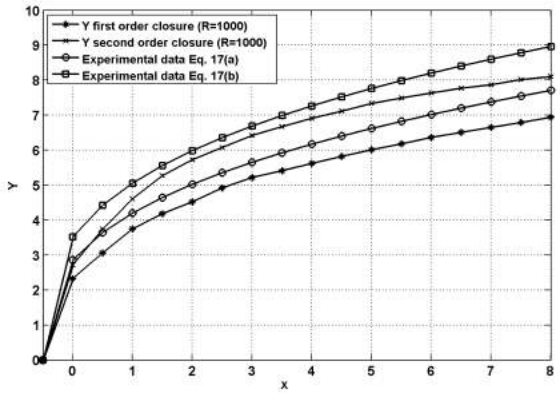

Figure 28: Liquid penetration obtained with the QME solver compared with the first order closure and with the experimental results.

flux lift up. Such qualitative validation of QME results is also confirmed in Figure 28 where a good agreement with respect to the experimental results is now recovered in terms of penetration with an effective deviation ξ=8%. The relative improvement in terms of penetration obtained through the turbulent liquid flux is thus higher respect to the previous test case and it is due to the leading importance of drag and pressure gradient effects in Equation 14 that have been correctly modelled. Thus, the QME solver has been validated also in a high density ratio environment like the one normally investigated in the aeroengine combustors leading to a strong improvement in the liquid distribution prediction.

4. CONCLUSIONS

This research activity was carried out with the main aim of developing an innovative CFD solver for the analysis of complex air assisted atomizers lean burn injection systems in the framework of the open-source suite OpenFOAM. The proposed solver is an improvement of the Eulerian two-phase solver, implemented in the Eulerian Lagrangian Spray Atomization (ELSA) model for the dense spray region, to include turbulent liquid flux effects. Considering the flow field characteristics of the lean injection modules and exploiting the Eulerian-Lagrangian results available for a realistic injection system, the unsuitability of first order closure has been verified in presence of a slip velocity between liquid and gas.

Therefore, a novel second order closure, where one equation is solved for each component of the

turbulent liquid flux, was proposed and integrated both with the liquid volume fraction and with the liquid /gas interface density equations. The approach proposed here presents an original splitting of the turbulent liquid flux in two parts. The drift flux is modelled according to a diffusion process and the slip liquid flux is represented by a particular transport equation where the effects of drag, body forces and pressure gradient have been considered. Such choice leads to a robust method able to introduce the leading phenomena directly linked to slip motion with strong advantages with respect to first order model. Furthermore, exploiting the definition of the liquid/gas interface density, it is able to reliably describe a polydisperse spray without any assumption in terms of shape for the liquid phase.

Thus, this QME model is actually applicable to simulate the injection from inside the injector to the final spray. In addition, this approach fills the gap between single Eulerian mixture flow and fully two-phase Eulerian-Eulerian approaches with the benefit to be applicable for all range of liquid and volume fraction addressing both dense and dispersed flows.

Solver capabilities have been tested in a jet in crossflow test case with a direct validation against both experimental data and R results from (Herrmann et al., 2011; Herrmann, 2010) as well as first order solver data. Such test case is extremely challenging since all the relevant physical two-phase regimes, from pure liquid to dispersed droplets, should be accounted for. Improvements in terms of liquid distribution have been obtained with respect to the first order solver both at intermediate and high density ratio. The agreement with experimental data was very good in the second test conditions where the effects of drag and pressure gradient in the equation of slip turbulent flux are higher than the test with R=10.

Acknolewdgements

Authors gratefully acknowledge Prof. Bruno Facchini for his useful suggestions and AvioAero for the permission of using PERM geometry.

REFERENCES

References

Acharya, S., Tyagi, M., Hoda, A., 2012. Flow and heat transfer predictions for film-cooling. Ann. NY Acad. Sci. 934 38, 110–125.

Andreini, A., Bianchini, C., Caciolli, G., Facchini, B., Giusti, A., Turrini, F., 2014a. Multi-coupled numerical analysis of advanced lean burn injection systems, in: Proc. ASME Turbo Expo.

Andreini, A., Bianchini, C., Facchini, B., Giusti, A., Turrini, F., 2013. A multi-coupled eulerian-lagrangian solver for airblast injectors including liquid film evolution and primary breakup - application. Proceedings of the ILASS-Europe .

Andreini, A., Caciolli, G., Facchini, B., Picchi, A., Turrini, F., 2014b. Experimental investigation of the flow field and the heat transfer on a scaled cooled combustor liner with realistic swirling flow generated by a lean-burn injection system. Journal of Turbomachinery 137.

Bailly, P., Champion, M., Garréton, D., 1997. Counter-gradient diffusion in a confined turbulent premixed flame. Physics of Fluids (1994-present) 9, 766–775.

Beau, P., 2006. Modelisation de l'atomisation d'un jet liquide. Application aux sprays Diesel. Ph.D. thesis. University of Rouen, France.

Beau, P., Funk, M., Lebas, R., Demoulin, F., 2005. Applying Quasi-Multiphase Model to Simulate Atomization Processes in Diesel Engines: Modeling of the Slip Velocity. Technical Report 2005-01-0220. SAE International.

Bellofiore, A., Cavaliere, A., Ragucci, R., 2007. Air density effect on the atomization of liquid jets in crossflow. Combustion Science and Technology 179, 319–342. doi:10.1080/00102200600809563.

Bianchini, C., Andrei, L., Andreini, A., Facchini, B., 2013. Numerical Benchmark of Nonconventional RANS Turbulence Models for Film and Effusion Cooling. Journal of Turbomachinery 135. URL: http://dx.doi.org/10.1115/1.4007614, doi:10.1115/1.4007614.

Boivin, M., Simonin, O., Squires, K.D., 2000. On the prediction of gas-solid flows with two-way coupling using large eddy simulation. Physics of Fluids 12, 2080–2090.

Borghi, R., Vallet, A., 1999. Modelisation eulerienne de l'atomisation d'un jet liquide. Comptes Rendus de l'Academie des Sciences - Series IIB - Mechanics-Physics-Astronomy 327, 1015–1020. doi:10.1016/S1287-4620(00)87013-1.

Brown, C., McDonell, V., 2006. Near field behaviour of a liquid jet in a crossflow. ILASS Americas, 19th Annual Conference on Liquid Atomization and Sprays systems, Toronto, Canada .

Buelow, P., Williams, B., Bretz, D., Spooner, M., Mohamed, C., Gill, H., 2006. Lean direct injection atomizer for gas turbine engines. Google Patents.

Chassaing, P., 2001. The modeling of variable density turbulent flows. a review of first-order closure schemes. Flow, turbulence and combustion 66, 293–332.

Chrigui, M., Sadiki, A., Batarseh, F.Z., Roisman, I., Tropea, C., 2008. Numerical and experimental study of spray produced by an airblast atomizer under elevated pressure conditions, in: Proc. ASME Turbo Expo, pp. 1011–1019.

Cooper, J., Duncan, B., Hura, H., Lohmueller, S., Mongia, H., Sabla, P., 2002. Fuel nozzle assembly for reduced exhaust emissions. Google Patents.

Demoulin, F., Beau, P., Blokkeel, G., Mura, A., Borghi, R., 2007. A new model for turbulent flows with large large density fluctuations: application to liquid atomization. Atomization and Sprays 17, 315–345. doi:10.1615/AtomizSpr.v17.i4.20.

Demoulin, F.X., Reveillon, J., Duret, B., Bouali, Z., Desjonqueres, P., Menard, T., 2013. Toward using Direct Nu-

merical Simulation to improve primary break-up modeling. Atomisation and Sprays 23, 957–980.

Deutsch, E., Simonin, O., 1991. Large eddy simulation applied to the motion of particles in stationary homogeneous fluid turbulence. Turbulence Modification in Multiphase Flows-ASME FED 110.

Dumouchel, C., 2008. On the experimental investigation on primary atomization of liquid streams. Experiments in Fluids 45, 371–422.

Elshamy, O.M., Jeng, S.M., 2005. Study of liquid jet in crossflow at elevated ambient pressures. Proceedings of the ILASS Americas, 18th Annual Conference on Liquid Atomization and Spray Systems .

Foust, M., Mongia, H., 2007. Method and apparatus for controlling combustor emissions. Google Patents.

Fox, R.O., Laurent, F., Massot, M., 2008. Numerical simulation of spray coalescence in an Eulerian framework: Direct quadrature method of moments and multi-fluid method. Journal of Computational Physics 227, 3058–3088.

Freitag, S., Hassa, C., 2008. Spray characteristics of a kerosene jet in cross flow of air at elevated pressure, in: Proceedings ILASS-Europe.

Gicquel, L.Y.M., Staffelbach, G., Poinsot, T., 2012. Large Eddy Simulations of gaseous flames in gas turbine combustion chambers. Progress in Energy and Combustion Science 38, 782–817.

Giusti, A., 2013. Development of numerical tools for the analysis of advanced airblast injection systems for lean burn aero-engine combustors. Ph.D. thesis. Department of Industrial Engineering of University of Florence.

Hernandez, D., Lachaud, E., Noel, T., 2015. Multipoint injection device for a combustion chamber of a turbine engine. Google Patents.

Herrmann, M., 2010. Detailed numerical simulations of the primary atomization of a turbulent liquid jet in crossflow. ASME J. Gas Turb. Pwr 132, 061506.1–10.

Herrmann, M., Arienti, M., Soteriou, M., 2011. The impact of density ratio on the liquid core dynamics of a turbulent liquid jet injected into a crossflow. ASME J. Gas Turb. Pwr 133, 061501–9.

Hoda, A., Acharya, S., Tyagi, M., 2000. Reynolds stress transport model predictions and large eddy simulations for film coolant jet in crossflow, in: Proc. ASME Turbo Expo.

ICAO, 2010. Enviromental report, aviation and climate change. URL: http://www.icao.int/environmentalprotection/Documents/Publications/ENVReport2010.pdf.

Jasak, H., 1996. Error analysis and estimation for the finite volume method with applications to fluid flows. Ph.D. thesis. Imperial College, University of London.

Jasak, H., Weller, H.G., Nordin, N., 2004. In-cylinder CFD simulation using a C++ object-oriented toolkit. Technical Report. SAE Technical Paper.

Kern, M., Marinov, S., Merkle, K., Zarzalis, N., Peschiulli, A., Turrini, F., 2011. Characteristics of an ultra-lean swirl combustor flow by LES and comparison to measurements, in: Proc. ASME Turbo Expo, pp. 321–330.

Launder, B., Reece, G., Rodi, W., 1975. Progress in the development of a reynolds-stress turbulence closure. Journal of fluid mechanics 68, 537–566.

Launder, B., Sharma, B., 1974. Application of the energy-dissipation model of turbulence to the calculation of flow near a spinning disc. Letters in heat and mass transfer 1, 131–137.

Laurent, F., Massot, M., 2001. Multi-fluid modelling of laminar polydisperse spray flames: origin, assumptions and comparison of sectional and sampling methods. Combustion Theory Modelling 5, 537–572. doi:10.1088/1364-7830/5/4/303.

Laurent, F., Massot, M., P., V., 2004. Eulerian multi-fluid modeling for the numerical simulation of coalescence in polydisperse dense liquid sprays. Journal of Computational Physics 194, 505 – 543. doi:http://dx.doi.org/10.1016/j.jcp.2003.08.026.

Lavergne, G., 2012. Fuel injection and spray evaporation. Lecture Series 2012-04, Von Karman Institute for Fluid Dynamics. .

Lebas, R., 2007. Modelisation Eulerienne de l'Atomisation Haute Pression. Influence sur la Vaporisation et la Combustion Induite. Ph.D. thesis. University of Rouen, France.

Lebas, R., Menard, T., Beau, P.A., Berlemont, A., Demoulin, F.X., 2009. Numerical simulation of primary break-up and atomization: DNS and modelling study. International Journal of Multiphase Flow 35, 247–260. doi:10.1016/j.ijmultiphaseflow.2008.11.005.

Li, S., Hsieh, S., Hsiao, G., Mongia, H., 2010. Pilot mixer for mixer assembly of a gas turbine engine combustor having a primary fuel injector and a plurality of secondary fuel injection ports. Google Patents.

Lubarsky, E., Zinn, B.T., Shcherbik, D., Bibik, O., Gopala, Y., 2012. Fuel Jet in Cross Flow-Experimental Study of Spray Characteristics. INTECH Open Access Publisher.

Marchisio, D.L., Fox, R.O., 2005. Solution of population balance equations using the direct quadrature method of moments. Journal of Aerosol Science 36, 43–73.

Marchisio, D.L., Pikturna, J.T., Fox, R.O., Vigil, R.D., Barresi, A.A., 2003. Quadrature method of moments for population-balance equations. AIChE Journal 49, 1266–1276.

Marinov, S., Kern, M., Merkle, K., Zarzalis, N., Peschiulli, A., Turrini, F., Sara, O., 2010. On swirl stabilized flame characteristics near the weak extinction limit, in: Proc. ASME Turbo Expo, pp. 259–268.

McGraw, R., 1997. Description of aerosol dynamics by the quadrature method of moments. Aerosol Science and Technology 27, 255–265.

Meier, U., Freitag, S., Heinze, J., Lange, L., Magens, E., Schroll, M., Willert, C., Hassa, C., Bagchi, I.K., Lazik, W., Whiteman, M., 2013. Characterization of Lean Burn Module Air Blast Pilot Injector With Laser Techniques. ASME J. Gas Turb. Pwr 135, 121508.1–121508.7. doi:10.1115/1.4025148.

Mongia, H., 2003. Taps - a 4th generation propulsion combustor technology for low emissions. The next 100 years, international air and space symposium and exposition. .

Riber, E., Moreau, M., Simonin, O., Cuenot, B., 2006. Development of Euler-Euler LES approach for gas-particle turbulent jet flow, in: ASME 2006 2nd Joint US-European Fluids Engineering Summer Meeting Collocated With the 14th International Conference on Nuclear Engineering, pp. 1663–1672.

Ruger, M., Hohmann, S., Sommerfeld, M., Kohnen, G., 2000. Euler/lagrange calculations of turbulent sprays: the effect of droplet collisions and coalescence. Atomization and Sprays 10.

Rusche, H., 2002. Computational Fluid Dynamics of dispersed two-phase flows at high phase fractions. Ph.D. thesis. Imperial College of London, England.

Simonin, O., 2000. Statistical and continuum modelling of turbulent reactive particulate flows. Lecture Series 1996-02, Von Karman Institute for Fluid Dynamics .

Smith, S.H., Mungal, M.G., 1998. Mixing, structure and scaling of the jet in crossflow. Journal of Fluid Mechanics 357, 83–122.

Stenzler, J.N., Lee, J.G., Santavicca, D.A., Lee, W., 2006. Penetration of liquid jets in a cross-flow. Atomization and Sprays 16.

Vallet, A., Burluka, A.A., Borghi, R., 2001. Development of a eulerian model for the atomization of a liquid jet. Atomization and Sprays 11, 619–642. doi:10.1615/AtomizSpr.v11.i6.20.

Williams, F., 1958. Spray Combustion and Atomization. Physics of Fluids 1, 541–545. doi:10.1063/1.1724379.

Wu, P., Kirkendall, K.A., Fuller, R.P., Nejad, A.S., 1997. Breakup processes of liquid jets in subsonic crossflows. Journal of Propulsion and Power 13, 64–73. doi:10.2514/2.5151.